Electronic Supplementary Information

A F-deficient and high-Mn ternary perovskite fluoride anode with a dominant conversion mechanism for advanced Li-ion batteries

Yongfa Huang, Rui Ding*, Danfeng Ying, Yuxi Huang, Caini Tan, Tong Yan, Xiujuan Sun, and Enhui Liu

Key Laboratory of Environmentally Friendly Chemistry and Applications of Ministry of Education, College of Chemistry, Xiangtan University, Hunan 411105, P.R. China

* E-mails: drm8122@163.com; drm8122@xtu.edu.cn (R. Ding);

Tel: +86 731 58292202; Fax: +86 731 58292251

Table of contents

Experimental section:

Preparation of KNCMF: The KNCMF materials were synthesized by one-pot solvothermal method based on the orthogonal experiment (**Table S1, S2**). Take the procedure of KNCMF-3# for an example. Firstly, 0.4 mmol of $NiCl_2 \cdot 6H_2O$, 0.4 mmol of $CoCl_2 \cdot 6H_2O$, 1.2 mmol of $MnCl_2 \cdot 4H_2O$, 4 mmol of $KF \cdot 2H_2O$ and 0.2 g of PVP-K30 were dissolved into the mixed solvents of 18 mL ethylene glycol and 18 mL of N-butanol, and then ultrasonically dispersed to an uniform mixture; Secondly, the mixture was poured into a 50 mL stainless steel Teflon reactor, and then placed in an oven under 180 ℃ for 24 h and allowed to cool down to room temperature; Finally, the precipitates were centrifuged three times with absolute ethanol and then dry in an oven under 100 ℃. The other samples were prepared as the above synthetic steps according to the specific orthogonal experimental conditions.

***Characterizations*:** The phases and crystal structures of samples were analysed by X-ray diffraction (XRD). The morphology and size of samples were characterized by scanning electron microscopy (SEM) and transmission electron microscopy (TEM). The microstructures of samples were measured by high-resolution TEM (HRTEM) and selected area electron diffraction (SAED). The element composition and distribution of samples were resolved by inductively coupled plasma-optical emission spectrometer (ICP-OES), X-ray energy dispersive spectra (EDS) and mapping. The chemical bonds and electronic structures of samples were checked by X-ray photoelectron spectra (XPS). The specific surface area and pore structure were tested by nitrogen

isothermal sorptions with Brunauer-Emmett-Teller (BET) and Barrett-Joyner-Halenda (BJH) methods, respectively.

***Electrochemical Measurements*:** The electrode fabrication is as follows: the mixture of active materials (for the cathode: $LiFePO_4$ (LFP); for the anode: KNCMF (1-10#)), acetylene black (AB) and polyvinylidene fluoride (PVDF) (7:2:1, w/w/w) were evenly mixed in N-methyl-2-pyrrolidone (NMP), which was coated onto an carbon-coated Al foil for cathode or Cu foil for anode, then dried in vacuum at 110 ℃ for 12 h. The coating mass of the active materials is controlled at around 1-3 mg cm^{-2}. Li-ion half cells were assembled into a 2032-type coin cells by using Li plate as a reference electrode and a counter electrode (RE/CE), and using an active material (LFP, KNCMF (1-10#)) as a working electrode (WE), 1 M $LiPF_6$ in ethylene carbonate (EC), ethyl methyl carbonate (EMC) and dimethyl carbonate (DMC) (1:1:1, v/v) with 1 wt% vinylene carbonate (VC) as the electrolytes, and a glass fiber as a separator. The LIBs were also assembled into 2032-type coin cells, the LFP electrode and the pre-lithiated KNCMF-3# anode (0.1 A g^{-1} for 4.5 cycles) were used as the cathode and anode respectively. All cells were assembled in an argon-filled glove box (MIKROUNA, O_2 and H_2O<0.1 ppm). All electrochemical tests were conducted on CHI 660E and Neware-CT-4008 working stations at room temperature (about 25 ℃) except the assigned tests under the low and high temperatures (-20 ℃ and 40 ℃). The chemicals, agents and materials for electrochemical tests are listed in the **Table S10**; The calculations for the specific capacity (C_m, mAh g^{-1}), energy density (E_m, Wh kg^{-1})

and power density (P_m, kW kg^{-1}) were conducted on the basis of **Equations (1), (2) and (3)**:

$C_m=Q/m$ S(1)

$E_m=C_mV$ S(2)

$P_m=3.6E_m/t$ S(3)

Where m, Q, V, and t are mass of active materials (g, for full cells, it refers to the total masses of active materials of anode and cathode), charge quantity (mAh), discharge platform voltage (V), and discharge time (s), respectively.

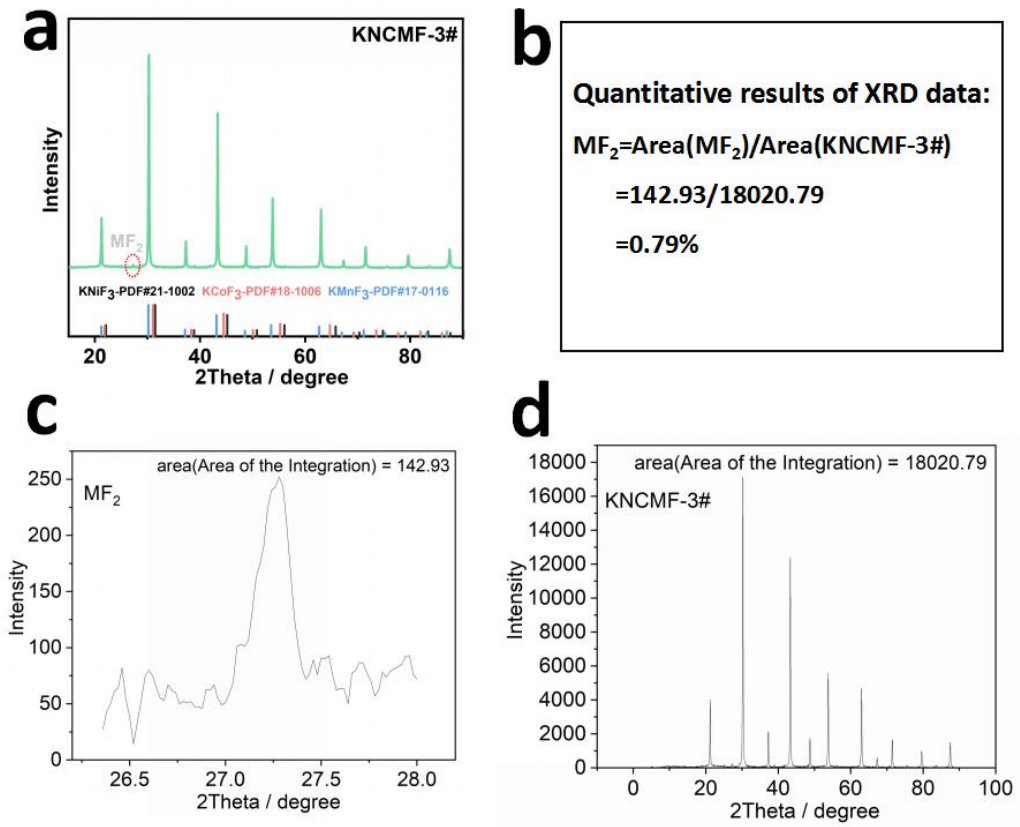

Figure S1 Quantitative analysis of XRD data of KNCMF-3# sample: XRD patterns (a), quantitative results (b), integrated areas of impurity MF_2 (c) and KNCMF-3# (d).

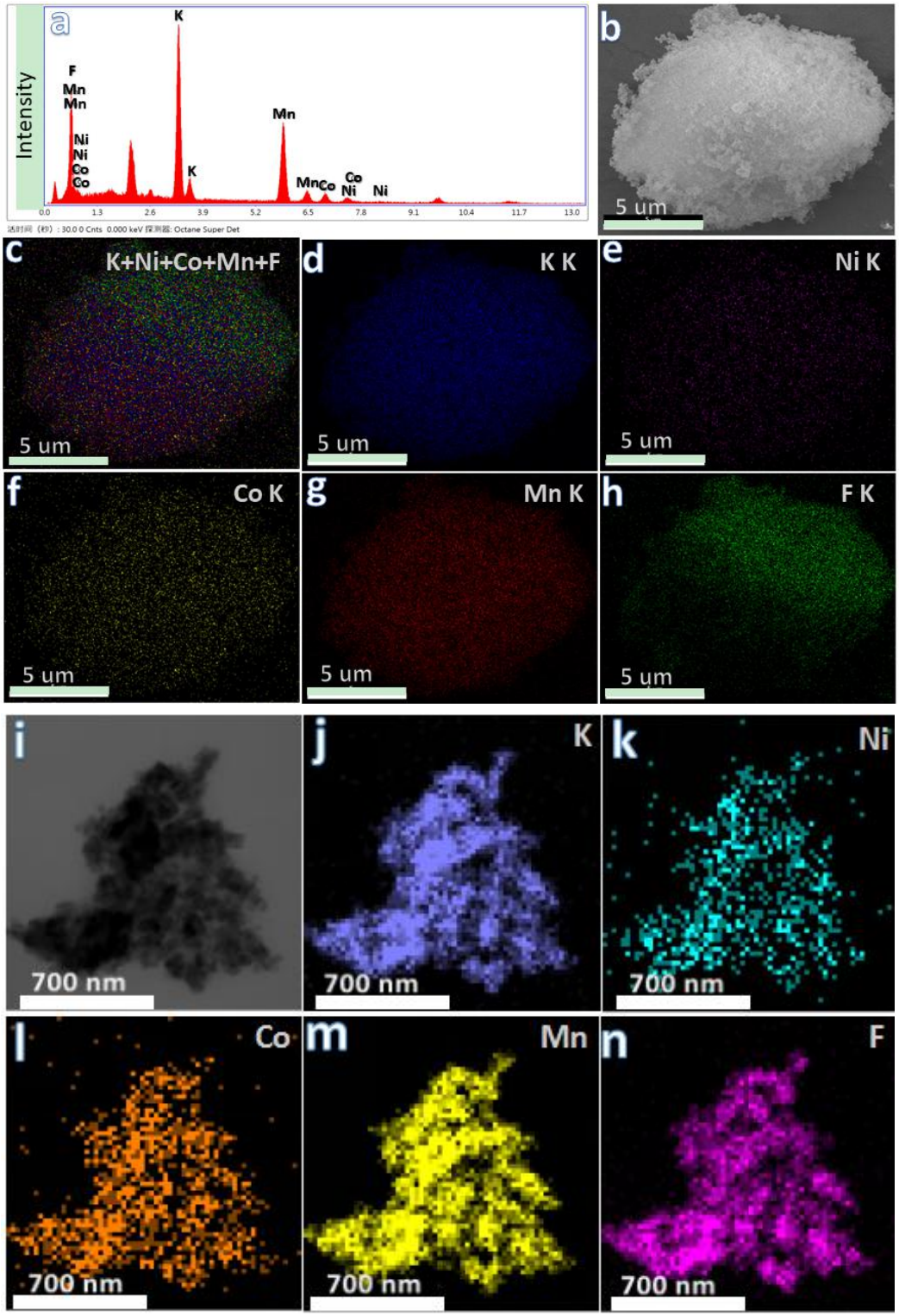

Figure S2 (a) EDS spectra and (b-n) element mapping from SEM/TEM images of KNCMF-3# sample.

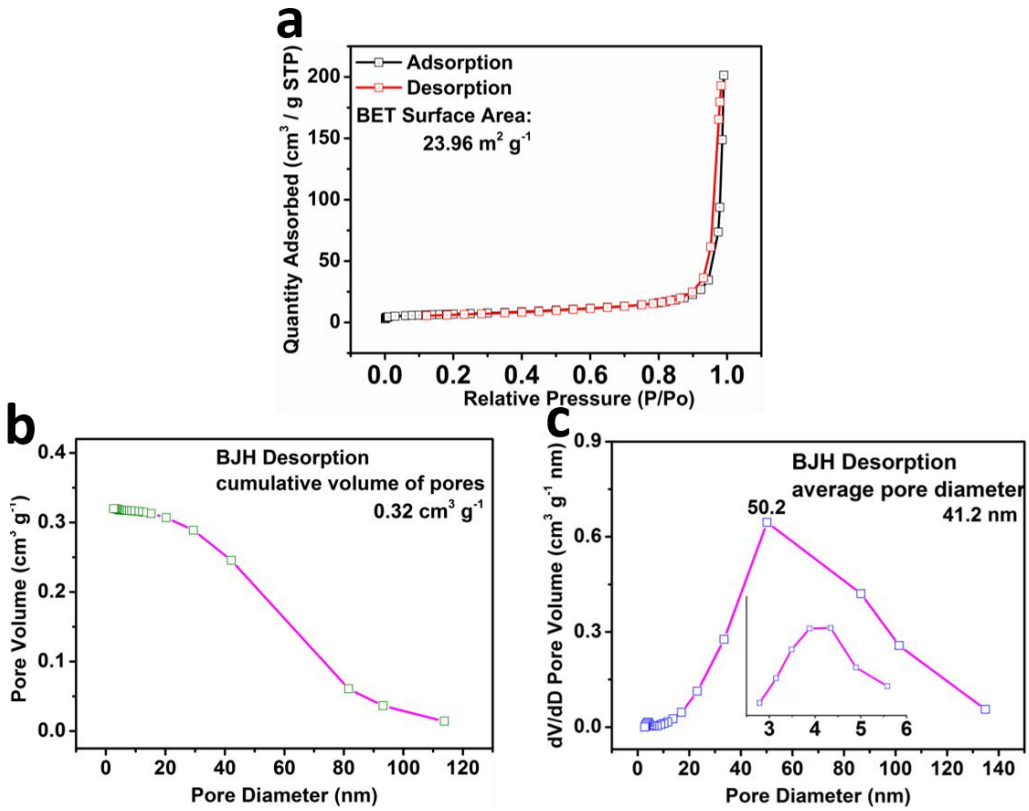

Figure S3 (a) BET, (b) pore volume and (c) pore size distribution of KNCMF-3# sample.

The N_2 sorption isotherms in Fig. S3 show the smaller hyshysteresis loop and the upswept line at the end of the isotherms, indicating the existence of mesopores and macropores. The small specific surface area and pore volume (23.96 m^2 g^{-1}, 0.32 cm^3 g^{-1}) indicate the limited sign of mesoporous features. The pore size mainly locates at 50.2 nm with the average pore diameter of 41.2 nm, which may be formed by the aggregations of particles.

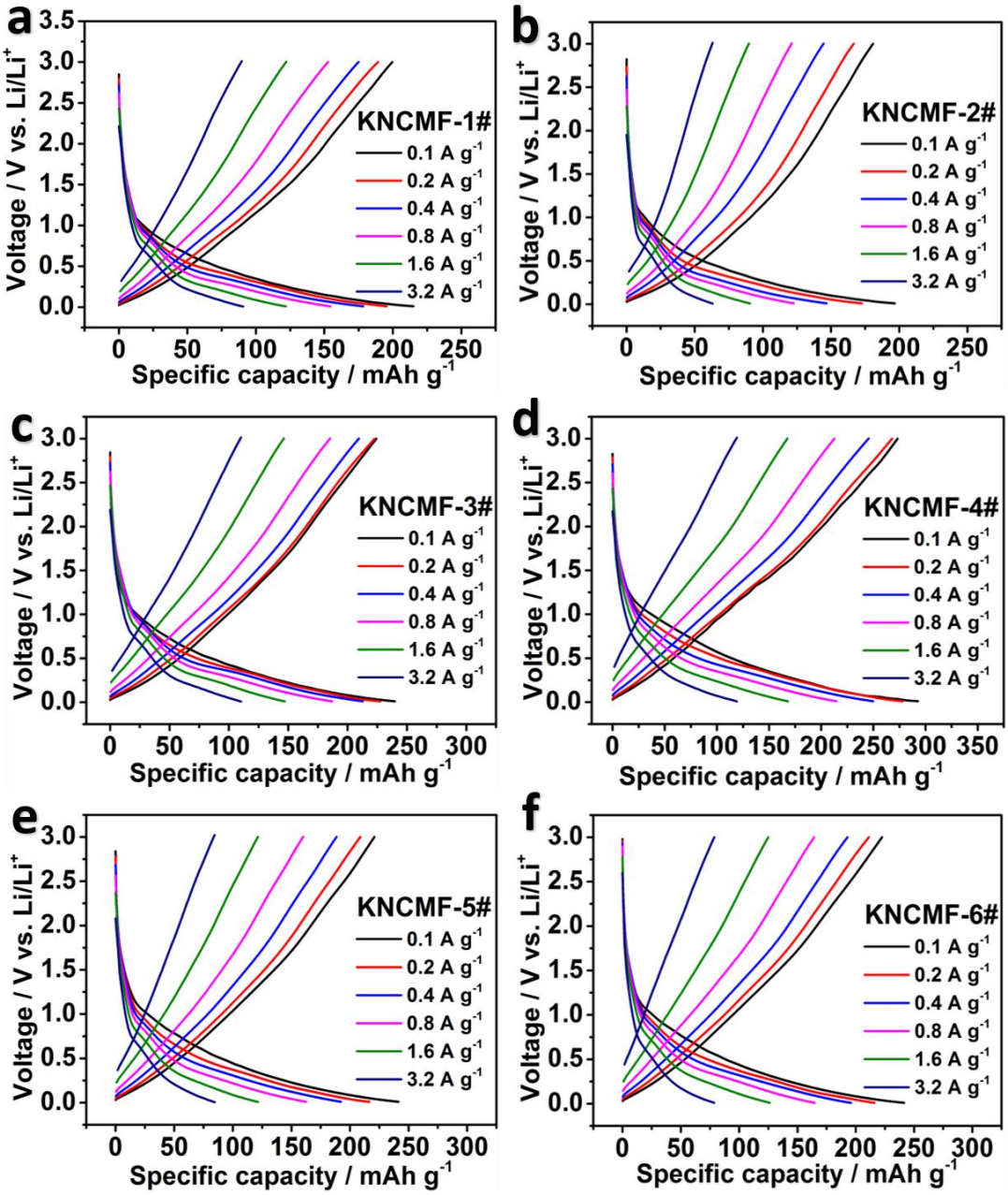

Figure S4 (a-f) GCD curves of KNCMF 1#~6# electrodes at 0.1-3.2 A g^{-1}.

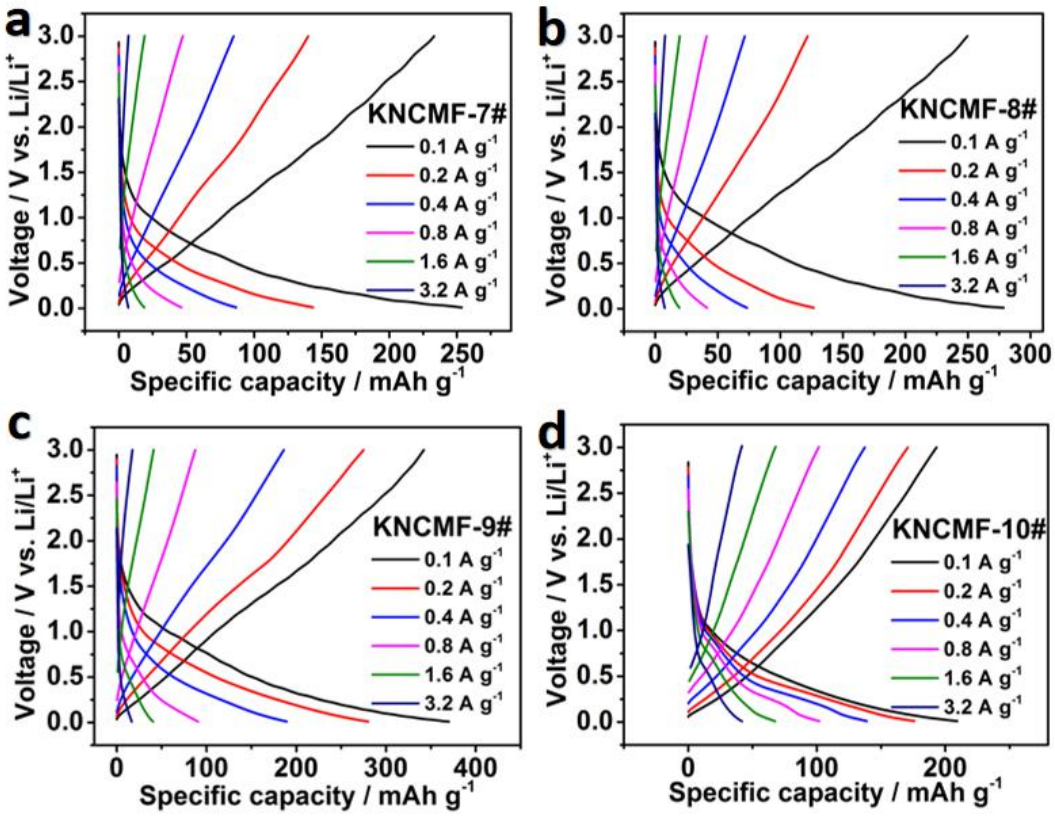

Figure S5 (a-d) GCD curves of KNCMF 7#~10# electrodes at 0.1-3.2 A g^{-1}.

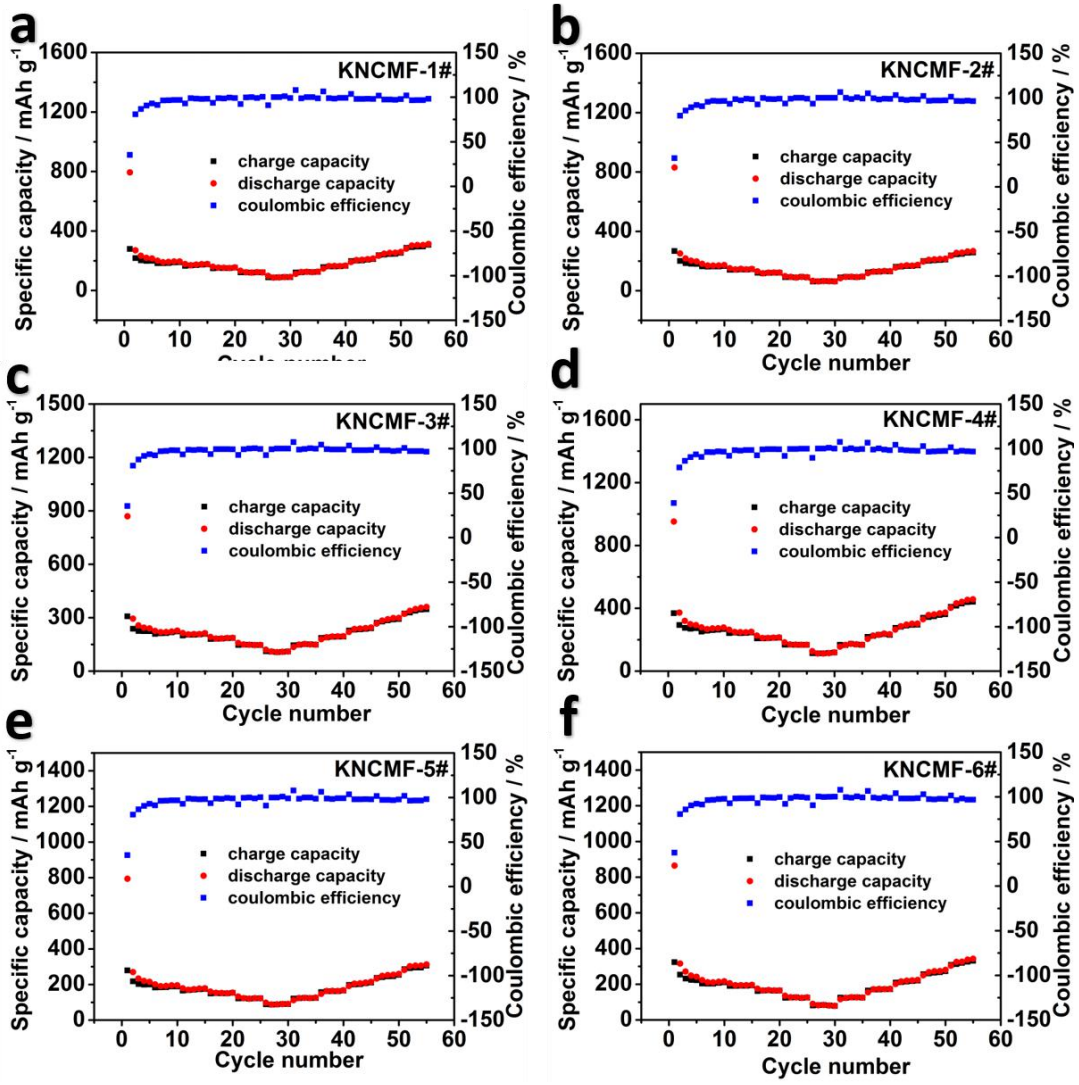

Figure S6 (a-f) rate performance and Coulombic efficiency of KNCMF 1#~6# electrodes at 0.1-3.2-0.1 A g^{-1}.

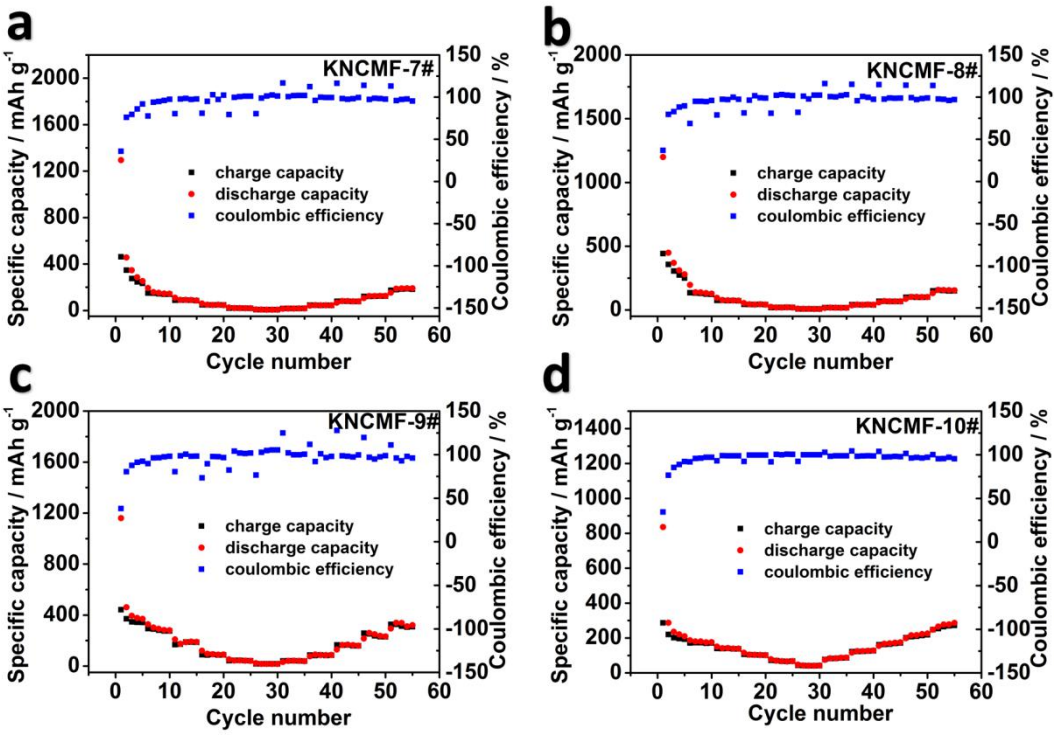

Figure S7 (a-d) rate performance and Coulombic efficiency of KNCMF 7#~10# electrodes at 0.1-3.2-0.1 A g^{-1}.

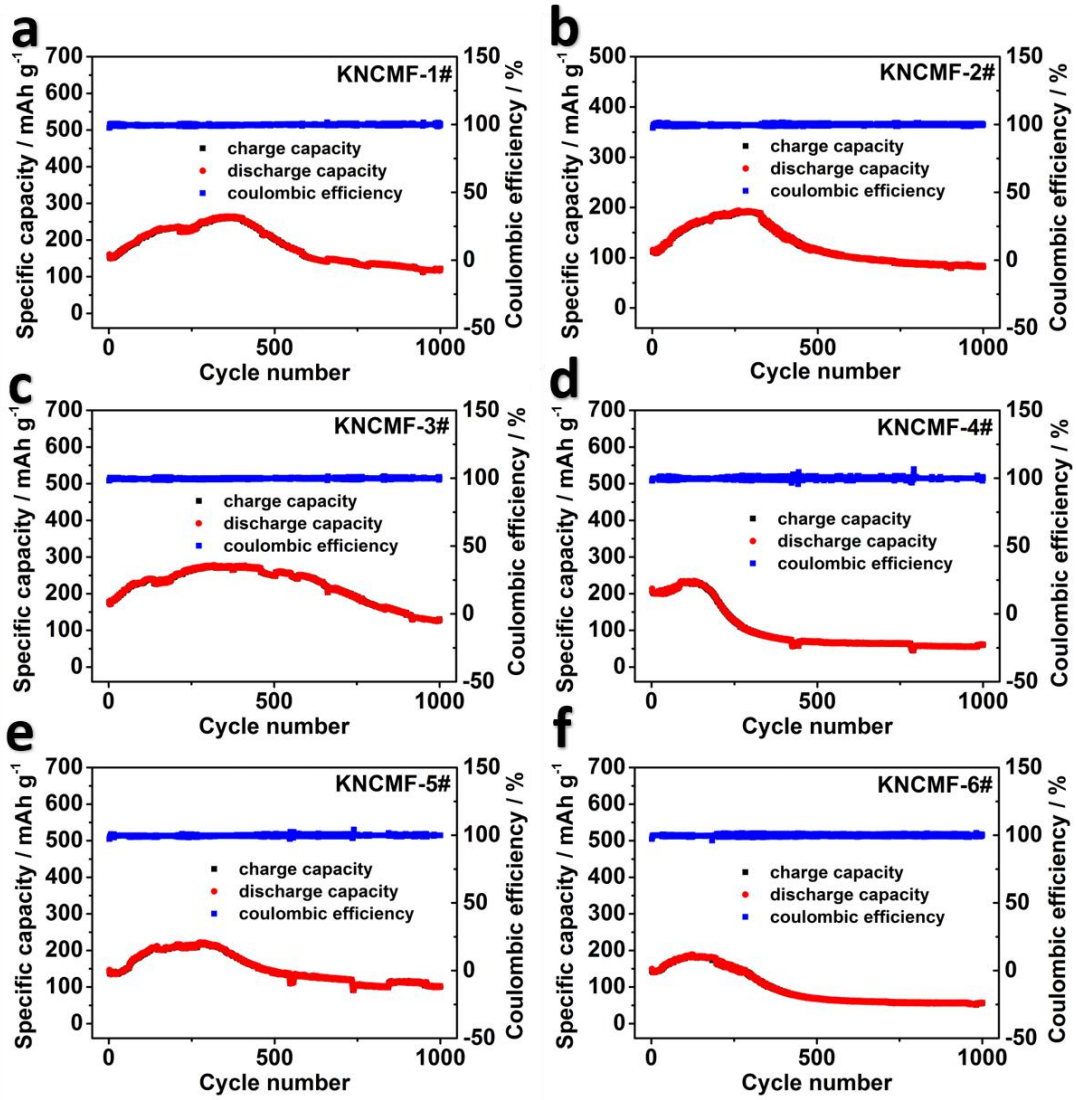

Figure S8 (a-f) cycling stability and Coulombic efficiency of KNCMF 1#~6# electrodes at 2 A g^{-1} for 1000 cycles.

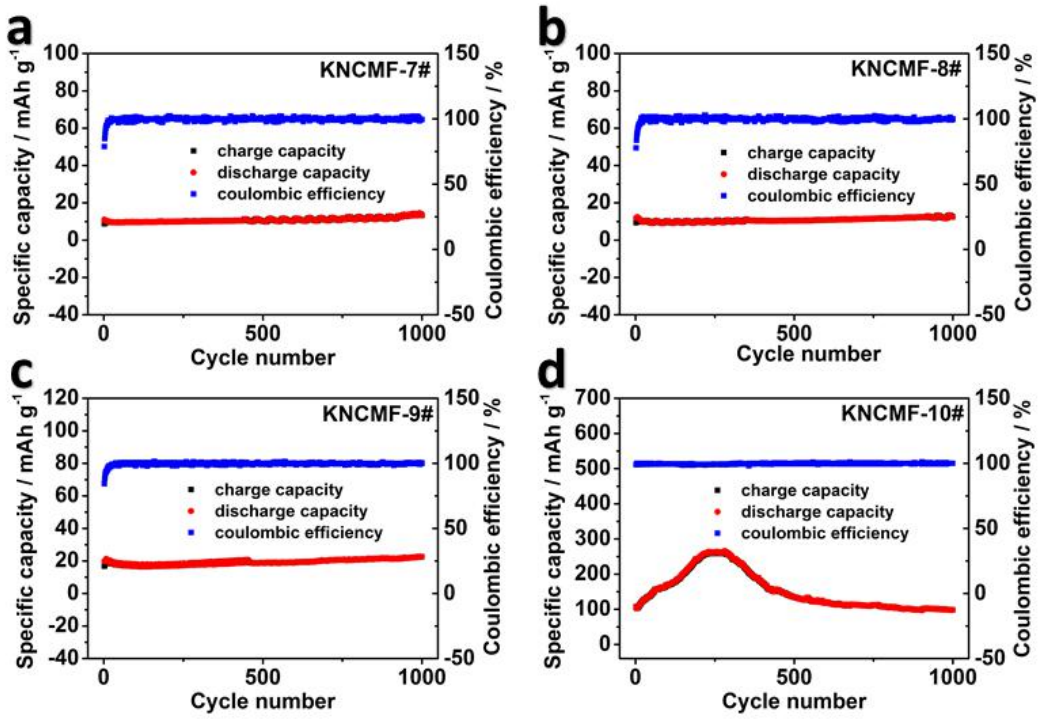

Figure S9 (a-d) cycling stability and Coulombic efficiency of KNCMF 7#~10# electrodes at 2 A g^{-1} for 1000 cycles.

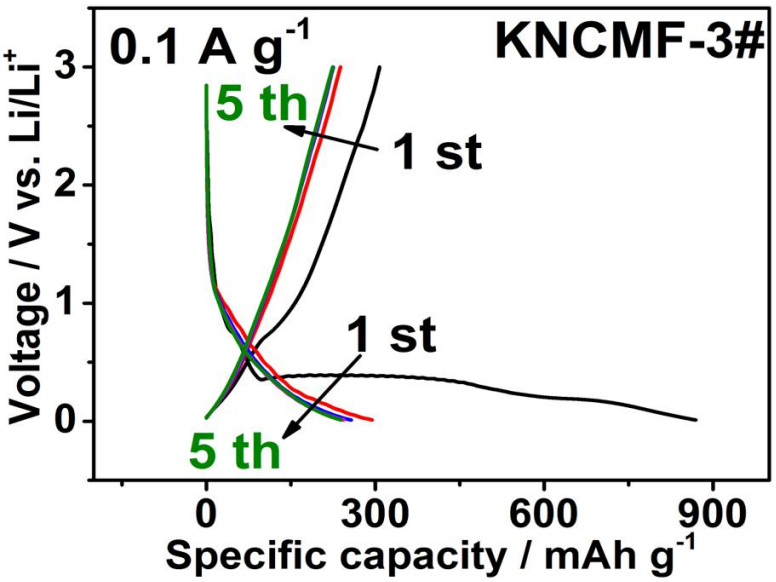

Figure S10 GCD curves of the first five cycles for KNCMF-3# electrode at 0.1 A g^{-1}.

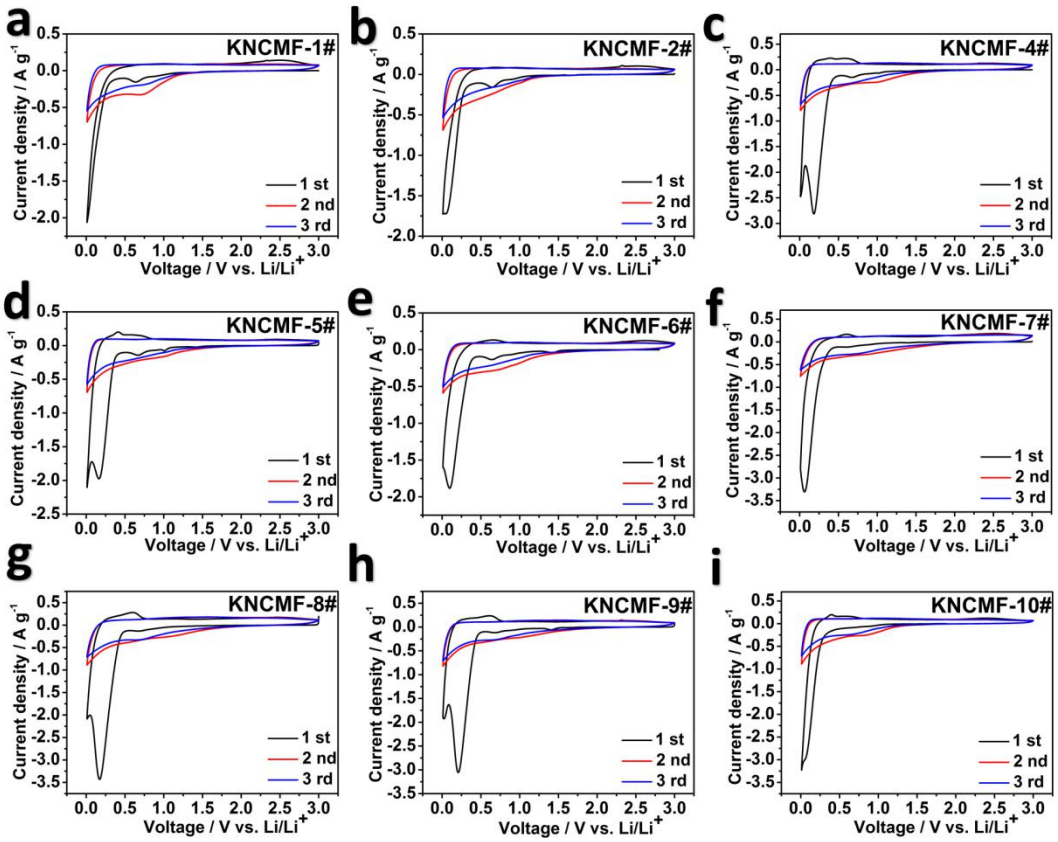

Figure S11 (a-i) CV plots of the first three cycles of KNCMF (1#, 2#, 4#, 5#, 6#, 7#, 8#, 9#, 10#) electrodes at 0.3 mV s^{-1}.

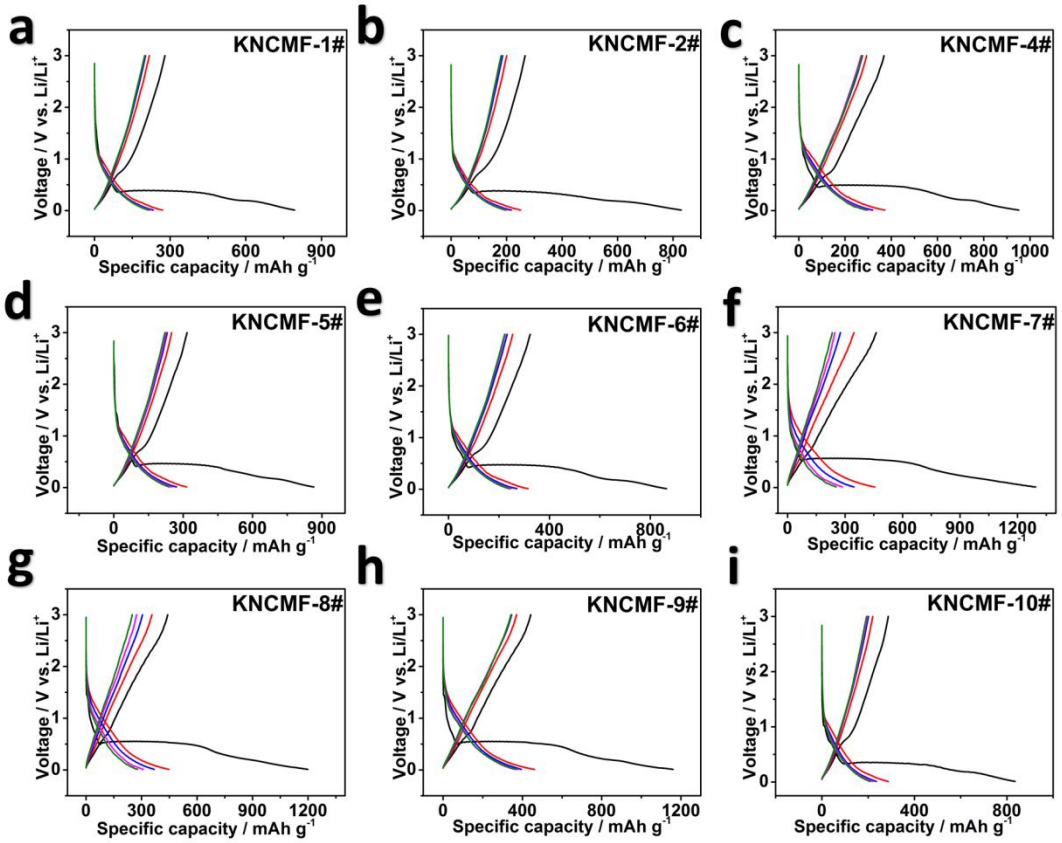

Figure S12 (a-i) GCD curves of the first five cycles for KNCMF (1#, 2#, 4#, 5#, 6#, 7#, 8#, 9#, 10#) electrodes at 0.1 A g^{-1}.

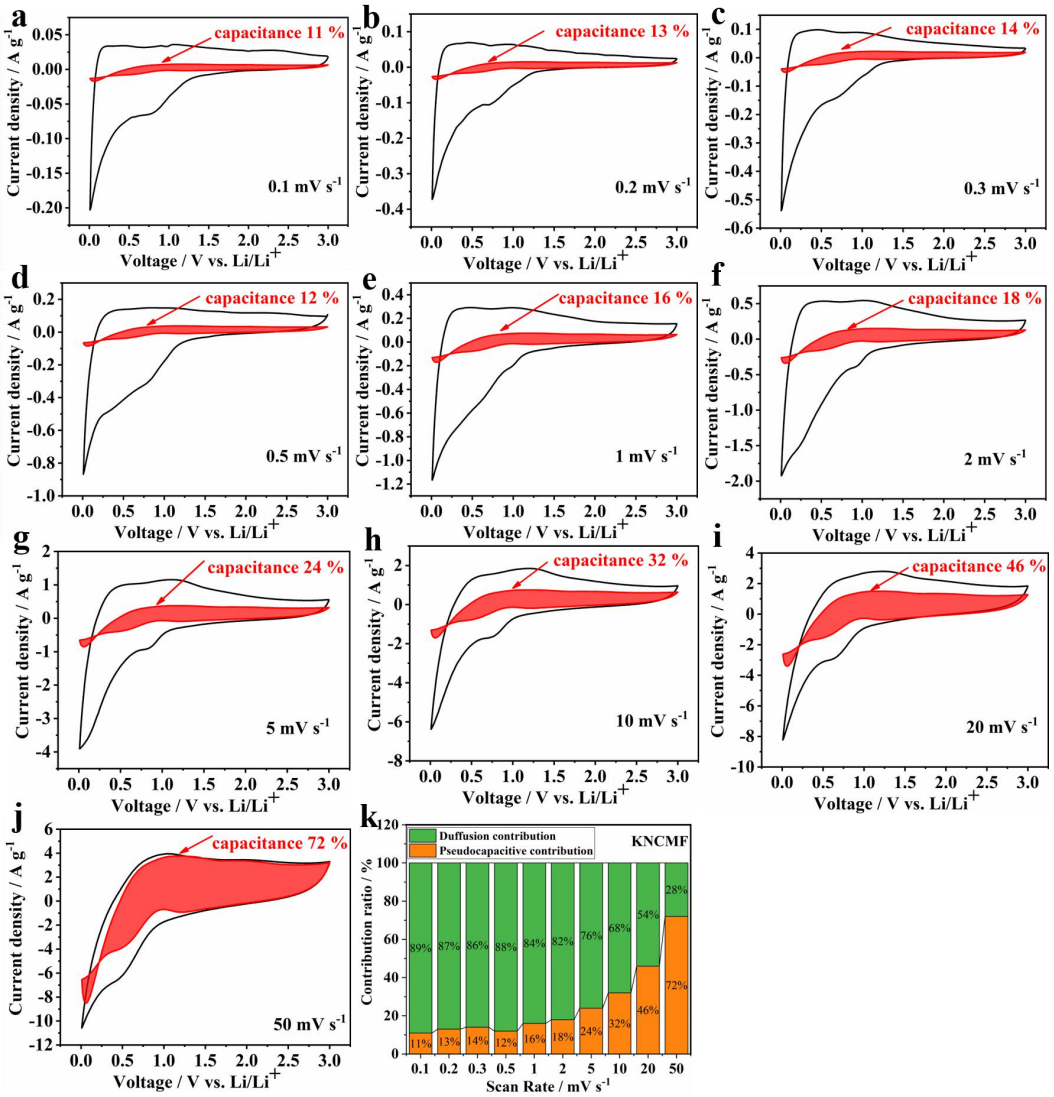

Figure S13 Pseudocapacitive contribution CV plots in shadow regions (a-j) and ratios (k) of the KNCMF-3# electrode.

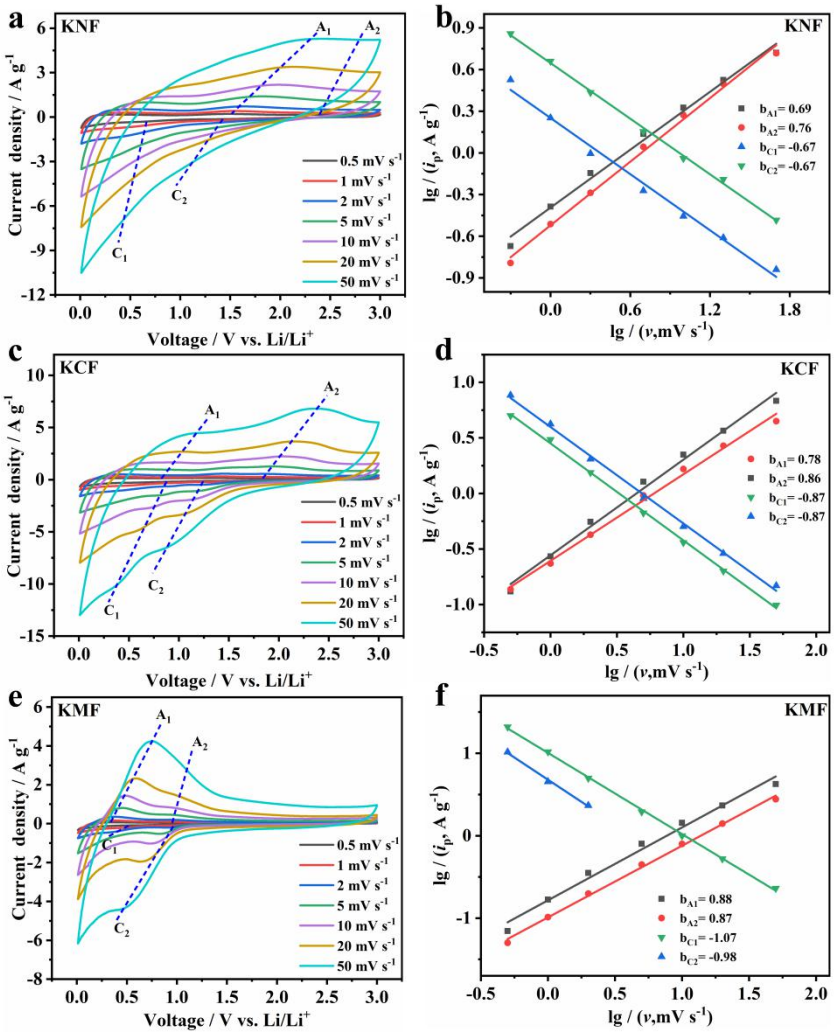

Figure S14 CV plots at 0.5~50 mV s^{-1} (a, c, e) and plots of lgi~lgv (b, d, f) of the KNF, KCF and KMF electrodes.

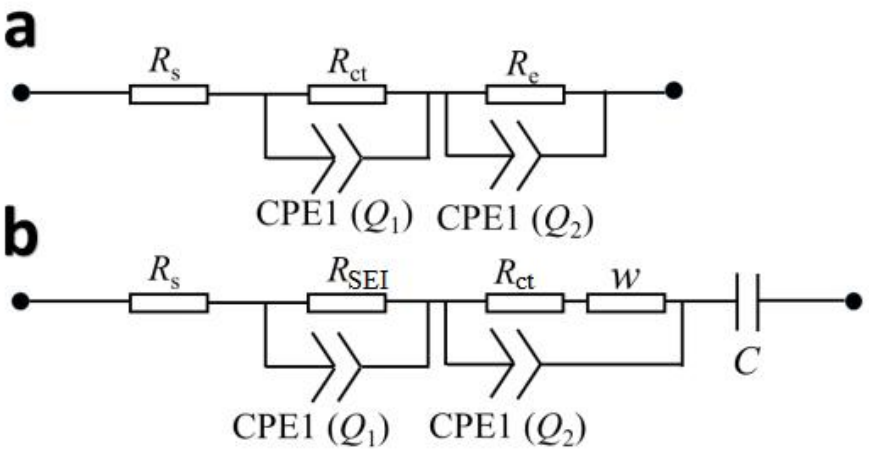

Figure S15 (a) the equivalent circuits used to fit the experimental Nyquist plots before and (b) after cycling of KNCMF-3# electrode.

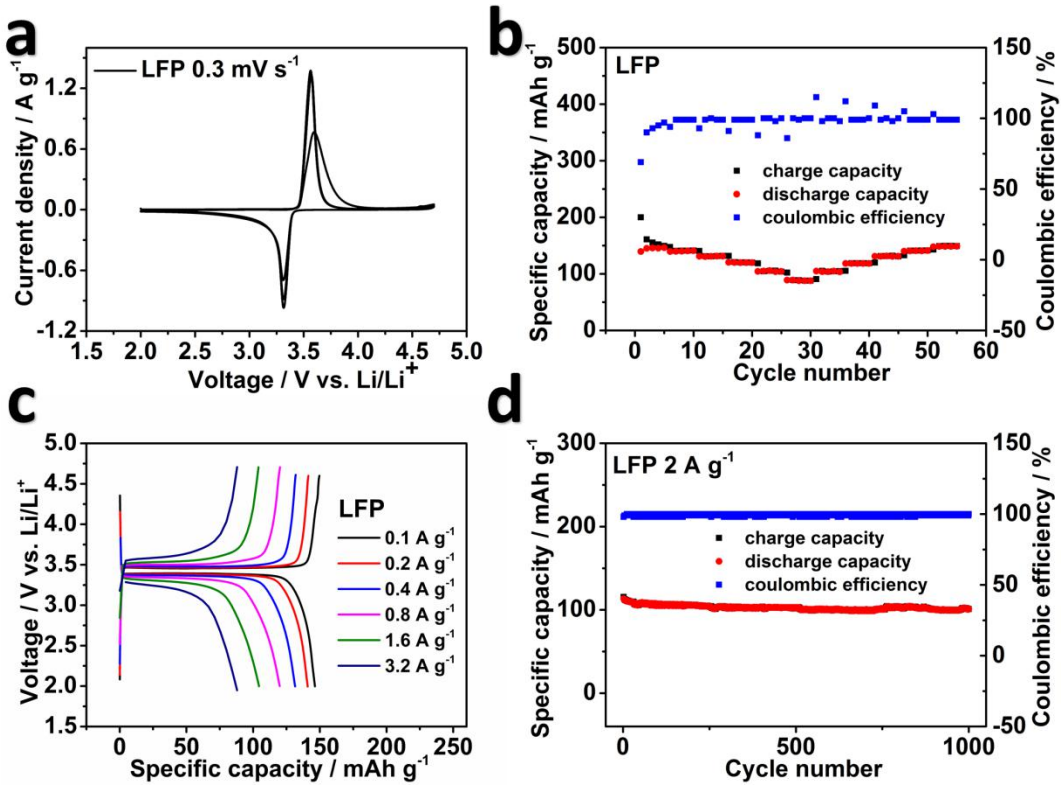

Figure S16 Performance of LFP electrode for Li-ion storage.

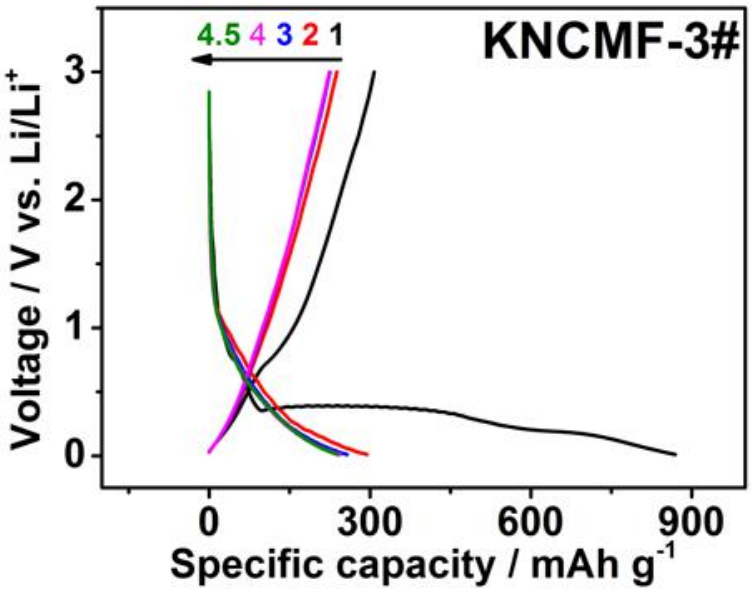

Figure S17 GCD curves of KNCMF-3# electrode at the pre-charged current density of 0.1 A g^{-1}.

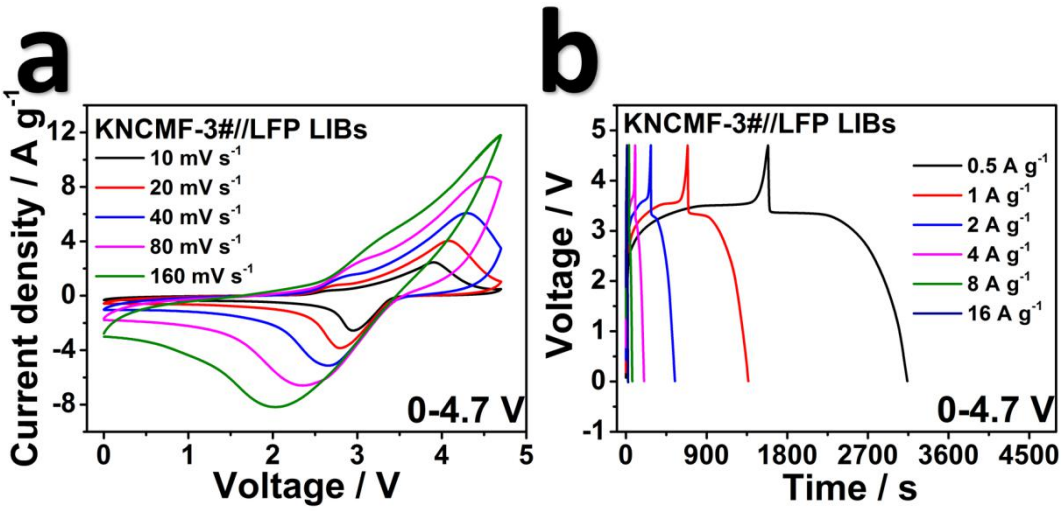

Figure S18 (a) CV plots of 4.7 V-KNCMF-3#//LFP LIBs, (b) GCD curves of 4.7 V-KNCMF-3#//LFP LIBs.

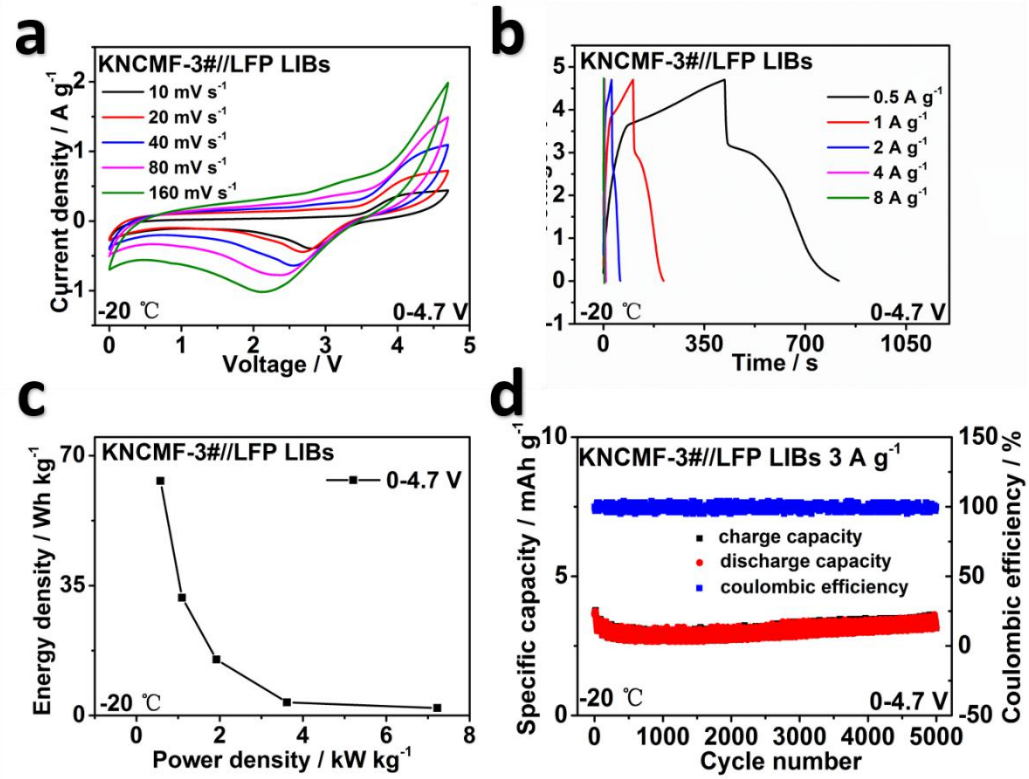

Figure S19 Performance of KNCMF-3#//LFP LIBs at the -20℃.

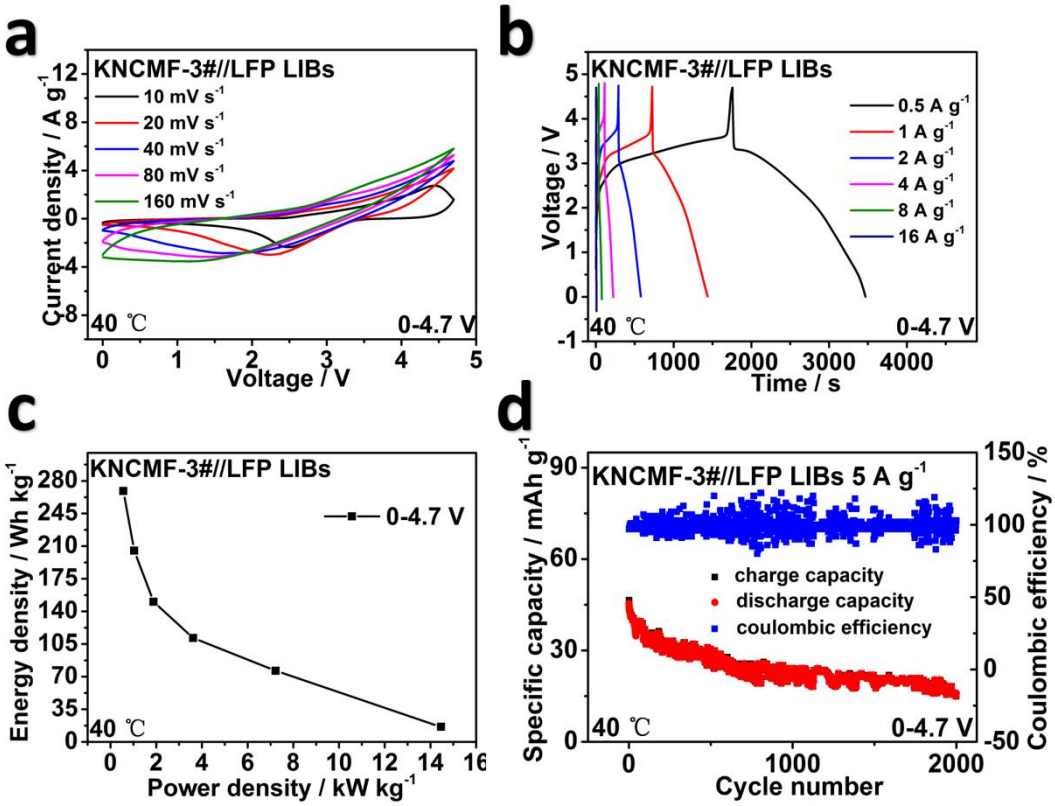

Figure S20 Performance of KNCMF-3#//LFP LIBs at the 40℃.

Figure S21 The experiment on lighting up a LED lamp at different time points based on the KNCMF//LFP LIB, (a) initial, (b) after 10 minutes, and (c) after 20 minutes.

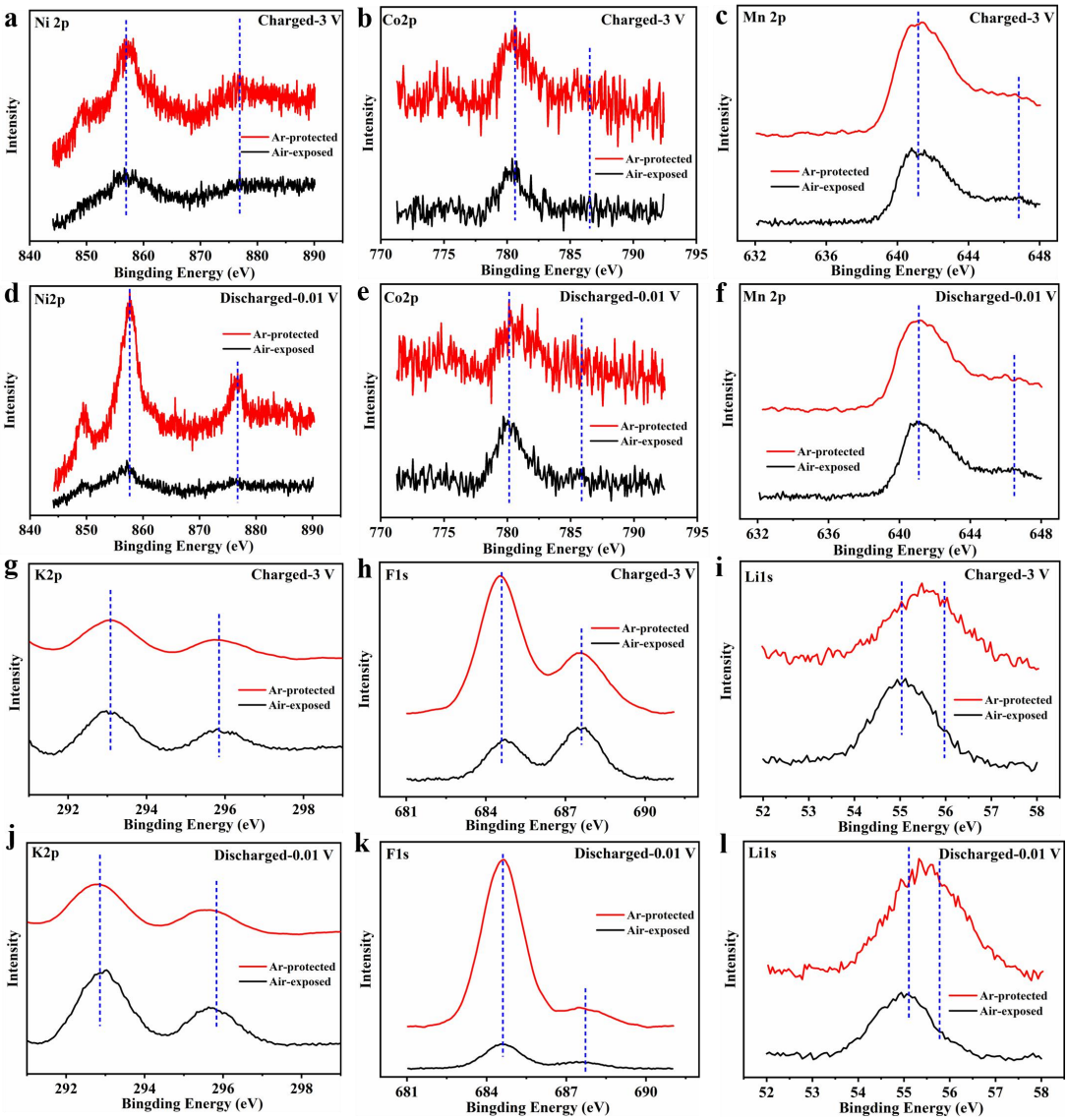

Figure S22 XPS control experiments (Ar-protected and Air-exposed) of the KNCMF-3# electrode in charged-3 V and discharged-0.01 V states for the first cycle.

XPS control experiments (Ar-protected and Air-exposed) of the KNCMF-3# charged/discharged samples have also conducted to examine the influence of aging time on the XPS results (Fig. S22), which show that the plots shapes and peaks binding energy of Ni2p, Co2p, Mn2p, K2p and F1s are basically same, although the light difference in peak binding energy of Li1s owing to the light difference of charge/discharge capacity and virable SEI thickness of the specific electrodes, showing that the aging time in air has a negligible influence on the XPS interpretation.

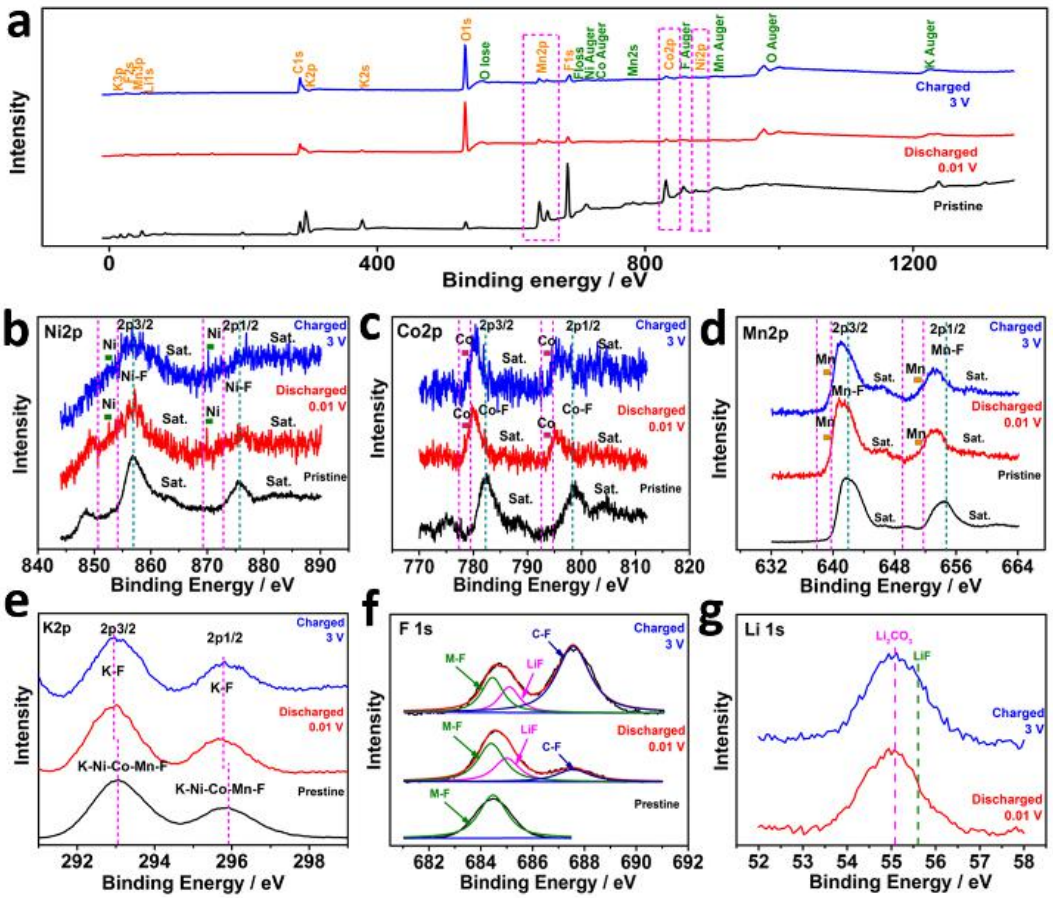

Figure S23 XPS spectra (Air-exposed) of the KNCMF-3# electrode in pristine, discharged -0.01 V and charged -3 V states for the first cycle at 0.05 A g^{-1}: (a) survey, (b) Ni2p, (c) Co2p, (d) Mn2p, (e) K2p, (f) F1s and (g) Li1s.

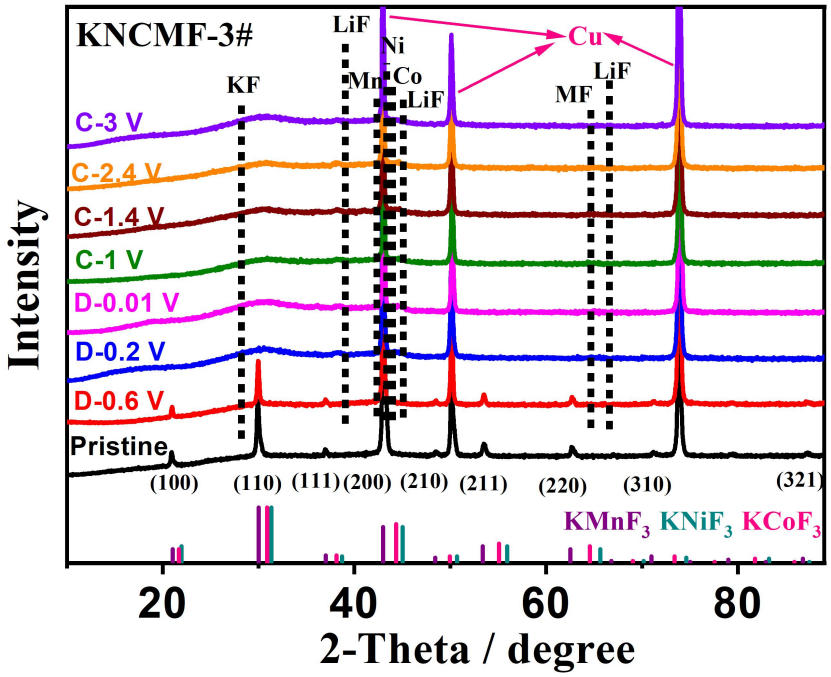

Figure S24 Ex-situ XRD plots in pristine and initial discharged/charged states (discharged-0.6 V, discharged-0.2 V, discharged-0.01 V, charged-1 V, charged-1.4 V, charged-2.4 V, charged-3 V) of the KNCMF-3# electrode.

(a)

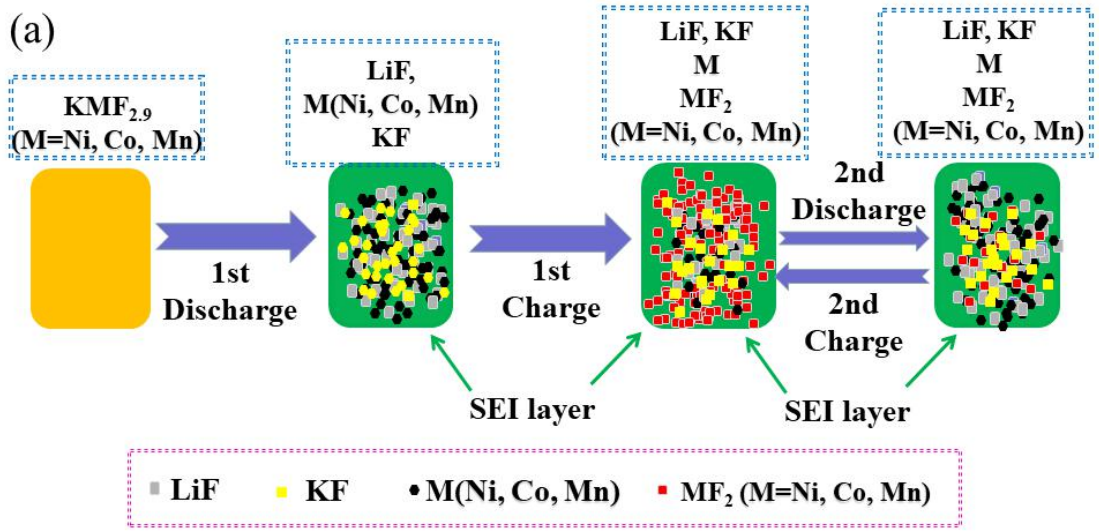

(b)

Phases	PDF Card	Crystal system	Space group	Cell (a x b x c) / Å
Ni	45-1027	Hexagonal	P63/mmc	2.651 × 2.651 ×4.343
Co	05-0727	Hexagonal	P63/mmc	2.503 ×2.503 ×4.061
Mn	17-0910	Tetragonal	I4/mmm	2.672 × 2.672 ×3.55
LiF	45-1460	Cubic	Fm-3m	4.027 × 4.027 ×4.027
NiF_2	24-0792	Tetragonal	P42/mnm	4.651 × 4.651× 3.084
CoF_2	38-0883	Cubic	Pa3	4.958 × 4.958× 4.958
MnF_2	34-1326	Tetragonal	P-42m	5.112 × 5.112× 5.256
KF	36-1458	Cubic	Fm-3m	5.348 × 5.348 × 5.348
$KNiF_3$	21-1002	Cubic	Pm-3m	4.013 × 4.013 × 4.013
$KCoF_3$	18-1006	Cubic	Pm-3m	4.071 × 4.071 × 4.071
$KMnF_3$	17-0116	Cubic	Pm-3m	4.189 × 4.189 × 4.189

(c)

$$\mathbf{xKMF_{2.92} + 1.92xLi^{+} + 1.92xe^{-} \rightarrow xKF + 1.92xLiF + xM} \quad \text{S(4)}$$

$$\mathbf{yM + 2yLiF \leftrightarrow yMF_2 + 2yLi^{+}} \quad \text{S(5)}$$

$$\mathbf{zLi^{+} + ze^{-} + xM/1.92xLiF \leftrightarrow xM/zLi/1.92xLiF} \quad \text{S(6)}$$

$$\mathbf{qLi^{+} + qe^{-} + xM/1.92xLiF \leftrightarrow qLi/xM/1.92xLiF} \quad \text{S(7)}$$

$$\mathbf{Li^{+} + electrolytes + e^{-} \leftrightarrow SEI\ films} \quad \text{S(8)}$$

Where M=Ni, Co and Mn; 0<x<1; 0<y, z, q<x.

Figure S25 (a) Schematics of reaction mechanisms of the KNCMF-3# electrode during the discharging/charging processes for the first two cycles for Li-ion storage; (b) Crystalline information of Ni, Co, Mn, LiF and KMF_3 (M=Ni, Co, Mn) phases; (c) The equations for reaction mechanisms of the KNCMF-3# electrode for Li-ion storag.

Level	Factors			
	mol ratio -A	Solvent (mL)-B	Temperature (℃)-C	Time (h)-D
1	1:2	EG+EA	160	6
2	1:2.5	EG+NPA	170	12
3	1:3	EG+NBA	180	24

Table S1 Orthogonal experimental design.

Samples	Conditions
1#	$A_1B_1C_1D_1$
2#	$A_1B_2C_2D_2$
3#	$A_1B_3C_3D_3$
4#	$A_2B_1C_2D_3$
5#	$A_2B_2C_3D_1$
6#	$A_2B_3C_1D_2$
7#	$A_3B_1C_3D_2$
8#	$A_3B_2C_1D_3$
9#	$A_3B_3C_2D_1$
10#	$A_1B_3C_3D_1$

Table S2 Synthesis conditions of KNCMF 1#~10#.

samples	Specific capacity / mAh g^{-1}						Cycle retention / %	Specific capacity after 1000 cycles / mAh g^{-1}
	0.1 (Ag^{-1})	0.2 (Ag^{-1})	0.4 (Ag^{-1})	0.8 (Ag^{-1})	1.6 (Ag^{-1})	3.2 (Ag^{-1})		
KNCMF-1#	215	195	178	154	122	91	76	122
KNCMF-2#	197	173	147	123	91	63	71	82
KNCMF-**3#**	**240**	**228**	**213**	**187**	**147**	**110**	**72**	**128**
KNCMF-4#	292	278	250	214	168	119	30	61
KNCMF-5#	215	195	178	154	122	91	69	101
KNCMF-6#	241	216	196	165	126	79	38	57
KNCMF-7#	253	144	87	46	19	7	118	13
KNCMF-8#	278	127	73	42	19	8	100	12
KNCMF-9#	370	280	189	91	40	17	115	23
KNCMF-10#	**209**	**176**	**139**	**102**	**68**	**42**	**91**	**98**

Table S3 Summary of performance of KNCMF electrodes

Test number	Experiment factor A (mol ratio)	B (solvent)	C (℃)	D (h)	Capacity (1A/g)	Rate (%)	Cycle retention (%)
1#	1(1:2)	1(EG+EA)	1(160℃)	1(6h)	215	42	76
2#	1	2(EG+NPA)	2(170℃)	2(12h)	197	32	71
3#	1	3(EG+NBA)	3(180℃)	3(24h)	240	46	72
4#	2(1:2.5)	1	2	3	292	41	30
5#	2	2	3	1	215	42	69
6#	2	3	1	2	241	33	38
7#	3(1:3)	1	3	2	253	3	118
8#	3	2	1	3	278	3	100
9#	3	3	2	1	370	5	115
Specific Capacity (mAh/g)	K1	652	760	734	800		
	K2	748	690	859	691		
	K3	901	851	708	810		
	k1	217.33	253.33	244.67	266.67		
	k2	249.33	230.00	286.33	230.33		
	k3	300.33	283.67	236.00	270.00		
	R	**83.00**	**53.67**	**41.67**	**36.33**		
Rate (%)	K1	120	86	78	89		
	K2	116	77	78	68		
	K3	11	84	91	90		
	k1	40.00	28.67	26.00	29.67	KNCMF	
	k2	38.67	25.67	26.00	22.67		
	k3	3.67	28.00	30.33	30.00		
	R	**36.33**	**3.00**	**4.33**	**7.33**		
Cycle retention (%)	K1	219	224	214	260		
	K2	137	240	216	227		
	K3	333	225	259	202		
	k1	73.00	74.67	71.33	86.67		
	k2	45.67	80.00	72.00	75.67		
	k3	111.00	75.00	86.33	67.33		
	R	**65.33**	**5.00**	**15.00**	**19.33**		
Specific capacity					A>B>C>D	A3B3C2D3(or D1)	
Rate retention					A>D>C>B	A1B1C3D3(or D1)	
Cycle retention					A>D>C>B	A3B2C3D1	
The optimal conditions					**A1B3C3(D1 or D3)**		
Selected optimal conditions					**A1B3C3D3**		

Table S4 Orthogonal experimental analysis results of KNCMF electrodes

EIS parameters			
Before cycling		**After cycling**	
Model	**R(QR)(QR)**	**Model**	**R(QR)(Q(RW))C**
R_s **(Ω)**	3.348	R_s **(Ω)**	4.322
Q_1 **(S·sec^n)**	1.518×10^{-5}	Q_1 **(S·sec^n)**	8.806×10^{-6}
n_1	0.8523	n_1	0.9694
R_{ct} **(Ω)**	56.83	R_{SEI} **(Ω)**	3.793
Q_2 **(S·sec^n)**	6.698×10^{-4}	Q_2 **(S·sec^n)**	1.25410^{-3}
n_2	0.9538	n_2	0.4712
R_e **(Ω)**	1.195×10^{5}	R_{ct} **(Ω)**	41.23
χ^2	2.39×10^{-3}	W **(S·sec$^{0.5}$)**	0.03593
		C **(F)**	0.05372
		χ^2	9.56×10^{-4}

Table S5 EIS parameters of KNCMF-3# electrode before and after cycling.

Systems	Q_m (mAh g^{-1}, 0.1A/g)		m_+/m_-
	Positive electrode	Negative electrode	
	LFP	KNCMF- 3#	
KNCMF-3#//LFP LIBs	146	240	**1.6:1**

Table S6 Design of m_+/m_- ratios for KCMF-3#//LFP LIBs.

Systems	Voltage window	Energy density (Wh kg^{-1})	Power density (kW kg^{-1})	Cycles
KNCMF-3#//LFP LIBs	0-4.7 V	**270.5~35.9**	**0.63~11.6**	5 A g^{-1}/1000/**84.8%** 5 A g^{-1}/2000/**82.6%** 5 A g^{-1}/3000/**86.2%** 5 A g^{-1}/5000/**71.1%**

Table S7 Summary of performance of KNCMF-3#//LFP LIBs at room temperature (about 25 ℃).

LIBs Systems	Voltage window / V	Energy density / Wh kg^{-1}	Power density / kW kg^{-1}	Cycling behavior / retention%, repeated cycles current density	Refs.
$Li_{4/3}Ti_{5/3}O_4$//$LiNi_xCo_yMn_{1-x-y}O_2$	1.5-2.7	90	2.2	#	**S1**
$Li_4Ti_5O_{12}$-$Li_2Ti_3O_7$//$LiFePO_4$	1.9-2.5	75	0.048	#	**S2**
TiO_2 nanofiber//$LiMn_2O_4$	1.7-2.5	220	0.314	90%/700/0.3 A g^{-1}	**S3**
FeSb-TiC//$Li_{1+x}Mn_{1.5}Ni_{0.5}O_4$	0-5.0	260	0.127	68%/50/0.0365 A g^{-1}	**S4**
Graphene/Si multilayer// $LiNi_{1/3}Mn_{1/3}Co_{1/3}O_2$	3-4.3	156	0.03	70.4%/15/0.0375 A g^{-1}	**S5**
TiO_2 hollow nanofiber //$LiFePO_4$	0.9-2.5	165	0.16	88%/300/0.1 A g^{-1}	**S6**
Ni_3N nanosheets//$LiNi_{0.5}Mn_{1.5}O_4$	2.5-4.1	120	3.39	99%/250/1.4 A g^{-1}	**S7**
KNCMF-3#//LFP	**0-4.7**	**270.5-35.9**	**0.63-11.6**	**86%/3000/5 A g^{-1} 71%/5000/5 A g^{-1}**	**This work**

Table S8. A performance comparison of this work with some reported LIBs.

Systems	T (℃)	Voltage window	Energy density (Wh kg^{-1})	Power density (kW kg^{-1})	Cycles
KNCMF-3#//LFP LIBs	-20	0-4.7 V	**63.2~2**	**0.63~11.6**	3 A g^{-1}/1000/**78.1%** 3 A g^{-1}/2000/**78.1%** 3 A g^{-1}/3000/**84.4%** 3 A g^{-1}/5000/**86.8%**
	40	0-4.7 V	**268.5~16**	**0.57~14.5**	5 A g^{-1}/500/**64.8%** 5 A g^{-1}/1000/**50.4%** 5 A g^{-1}/1500/**42.3%** 5 A g^{-1}/2000/**35.2%**

Table S9 Summary of performance of KNCMF-3#//LFP LIBs at the -20 / 40 ℃.

LIBs	Working voltage/ V	Energy density/ Wh kg^{-1}	Power density/ kW kg^{-1}	Cycling behavior/ retention%, repeated cycles, current density	Refs
KNCF(1:6)//LFP	0-4.7	173-29	0.75-15.3	67% / 2000 / 2 A g^{-1}	S8
NNCF(1:1)//LFP	1~4.7	196.2~35.2	0.8~19.2	63% / 2000 / 3 A g^{-1}	S9
KZMF(1-3)//LFP	0.5-4.6	130.8~15.9	0.8~14.3	48% / 5000 / 5 A g^{-1}	S10
KNCMF-3#//LFP	**0~4.7**	**270.5~35.9**	**0.63~11.6**	**71% / 5000 / 5 A g^{-1}**	**This work**

Note: KNCF(1:6), NNCF(1:1), KZMF(1-3) and KNCMF-3# mean the materials of $K_{1.0}Ni_{0.1}Co_{0.9}F_{3.0}$, $Na_{0.85}Ni_{0.45}Co_{0.55}F_{3.56}$, $K_{1.1}Zn_{0.17}Mn_{0.83}F_{3.03}$ and $K_{1.00}Ni_{0.06}Co_{0.14}Mn_{0.80}F_{2.92}$ respectively.

Table S10. A performance comparison of this work with some reported perovskite fluorides anode materials for LIBs.

Materials, chemicals and reagents	Type or level	Company	Characteristics
$NiCl_2$•6H_2O	AR	SinoPharm	Purity≥98.0%
$CoCl_2$•6H_2O	AR	SinoPharm	Purity≥99.0%
$MnCl_2$•4H_2O	AR	SinoPharm	Purity≥99.0%
KF•2H_2O	AR	SinoPharm	Purity≥99.0%
PVP-K30	GR	SinoPharm	#
EG	AR	SinoPharm	Purity≥99.0%
EA	AR	SinoPharm	Purity≥99.7%
NPA	AR	SinoPharm	Purity≥99.0%
NBA	AR	SinoPharm	Purity≥99.5%
$LiFePO_4$	LFP-NCO	Aleees	D50: 4 ± 2 μm; Tab: 1 ± 0.2 g cm^{-3}; SSA: 13 ± 2 m^2 g^{-1}
AB	Battery grade	#	#
NMP	AR	Kermel	Purity≥99.0%
PVDF	Battery grade	#	#
Electrolytes	LBC-305-01	CAPCHEM	1 M $LiPF_6$/EC: EMC: DMC (1:1:1)/1% VC
Li plate	15.6*0.45 mm	China Energy	15.6*0.45 mm
Cu foil	200*0.015	GuangZhou JiaYuan	Total thickness: 15 μm; Weight: 87 g m^{-2}
Carbon coated-Al foil	222*0.015	GuagZhou NaNuo	Total thickness: 17 μm; Strength: 192 Ma
Glass microfiber filters	GF/D 2.7 μm 1823-025	Whatman	Diameter: 25 mm; Thickness: 675 μm; Weight: 121 g m^{-2}
Cell components	CR-2032	ShenZhen TianChenHe	#

Table S11. Chemicals, reagents and materials used in the study.

References

S1. N. Takami, H. Inagaki, Y. Tatebayashi, H. Saruwatari, K. Honda and S. Egusa, *J. Power Sources*, 2013, **244**, 469-475.

S2. G. N. Zhu, L. Chen, Y. G. Wang, C. X. Wang, R. C. Che and Y. Y. Xia, *Adv. Funct. Mater.*, 2013, **23**, 640-647.

S3. V. Aravindan, J. Sundaramurthy, P. S. Kumar, N. Shubha, W. C. Ling, S. Ramakrishna and S. Madhavi, *Nanoscale*, 2013, **5**, 10636-10645.

S4. Z. Moorhead-Rosenberg, E. Allcorn and A. Manthiram, *Chem. Mater.*, 2014, **26**, 5905-5913.

S5. L. W. Ji, H. H. Zheng, A. Ismach, Z. K. Tan, S. D. Xun, E. Lin, V. Battaglia, V. Srinivasan and Y. G. Zhang, *Nano Energy*, 2012, **1**, 164-171.

S6. X. Zhang, V. Aravindan, P. S. Kumar, H. Liu, J. Sundaramurthy, S. Ramakrishna and S. Madhavi, *Nanoscale*, 2013, **5**, 5973-5980.

S7. M. S. Balogun, Y. X. Zeng, W. T. Qiu, Y. Luo, A. Onasanya, T. K. Olaniyi and Y. X. Tong, *J. Mater. Chem. A*, 2016, **4**, 9844-9849.

S8. Q. L. Xu, R. Ding, W. Shi, D. F. Ying, Y. F. Huang, T. Yan, P. Gao, X. J. Sun and E. H. Liu, *J. Mater. Chem. A*, 2019, **7**, 8315-8326.

S9. W. Shi, R. Ding, Q. L. Xu, T. Yan, Y. X. Huang, C. N. Tan, X. J, Sun, P. Gao and E. H. Liu, *Chem. Commun.*, 2019, **55**, 6739-6742.

S10. D. F. Ying, Q. L. Xu, R. Ding, Y. F. Huang, T. Yan, Y. X. Huang, C. N. Tan, X. J. Sun, P. Gao and E. H. Liu, *Chem. Eng. J.*, 2020, **388**, 124154.